Case study of the Ar^{9+}-He collision system at low velocity

S. Bliman,[1] R. Bruch,[2] M. Cornille,[3,*] A. Langereis,[4] and J. Nordgren[4]

[1]*Laboratoire de Spectroscopie Atomique et Ionique, UMR 8624, Batiment 350, Université Paris Sud, 91450 Orsay Cedex, France*
[2]*Department of Physics, University of Nevada, Reno, Nevada 89557*
[3]*LUTH Observatoire de Paris, FRE, 2462 CNRS, 92195 Meudon Cedex, France*
[4]*Department of Physics, Box 530, Uppsala University, S7521 Uppsala, Sweden*

The Ar^{9+}-He charge-exchange collision system is studied at low kinetic energy ($E = 2.25$ keV/amu), using two complementary instrumental techniques: x-ray and vacuum ultraviolet photon spectroscopy and Auger-electron spectroscopy. It is shown that single capture populates mostly $n=4$ and 5 in Ne-like argon $1s^2 2s^2 2p^5 nl$. The analysis and identification of the lines show the cascade population of $1s^2 2s 2p^6 3l$ states. These are not expected to be seen since in the entrance channel the projectile has the core $1s^2 2s^2 2p^5 \, ^2P^o_J$. They are identified by photon emission. Double capture populates mostly Na-like core excited states corresponding to the configurations $1s^2 2s^2 2p^5 3l5l'$. They are identified and it is seen that the continuum $2p^6 \, ^1S_0$ to which they Auger decay is the only one available in this case.

PACS number(s): 34.70.+e, 32.30.Jc, 32.90.+a

I. INTRODUCTION

Much effort has been devoted to the study of charge-exchange collisions in the low-energy range ($E < 25$ keV/amu). Knowledge of the cross sections appears to be useful for purposes such as evaluation of hot magnetically confined plasma impurity content and temperature estimates: A diagnostic technique based on the charge-exchange process between a fast neutral hydrogen beam and the plasma [1] is of current use in most tokamaks [2(a)]. Fast neutral lithium beams are also used to diagnose "scrape off" layer plasmas in some machines [2(b)]. Recently, astrophysical observations of x-ray emissions, identified as due to hydrogen-like oxygen and nitrogen ions, were performed. They were explained by charge exchange between highly ionized ions originating in solar wind and cometary atmospheres [3–5].

For single-electron capture (SC), the exit channels are, for example, lithiumlike ions for heliumlike projectiles in their ground states, and sodiumlike ions for neonlike projectiles, under the strict condition that there are no metastable fractions in the incident beams [6,7]. When considering projectiles in long-lived metastable states lying high above ground states, the exits are generally in the form of core excited ions, lithiumlike for heliumlike and sodiumlike for neonlike projectiles. In such cases, Auger stabilization is important.

For double-electron capture (DC), the availability of theoretical calculations is limited. They focus on the population of autoionizing states in collisions of bare and/or closed-shell ions [8–10].

It is also well known that in the neonlike isoelectronic sequence the $2p^5 3l$ configurations of highly charged ions have been the object of several investigations [11–13]. The interest in these ions was greatly stimulated by the possibility of obtaining laser action in some $3s \leftarrow 3p$ lines in the extreme ultraviolet region; the effort was focused on elements with atomic number $25 < Z < 37$ and particularly on Ge and

Se. Most of the fundamental spectroscopic investigations used either the beam-foil experimental technique, the observation of laser-produced plasmas, or fast capillary discharges and pinches [[11–13], and references therein]. For an element such as argon, these references give the experimental and calculated wavelengths for the $3s \leftarrow 3p$ and $3p \leftarrow 3d$ manifolds. In their tabulations, Bashkin and Stoner [14], Kelly [15], and Zhang *et al.* [16] give the wavelengths for the transitions of $2p^5 ns$ (with $n=4$) and $2p^5 nd$ (with $n=5$) to $2p^6 \, ^1S_0$. In the case of Ar^{9+}+He, the SC is expected to populate mostly $n=4$ and 5 in $2p^5 nl$. The most populated n (principal quantum number) [17] and l (orbital quantum number) [18,19] are estimated from scaling rules. When calculating the atomic features of highly charged Ar^{8+} one should include configurations such as $1s^2 2s 2p^6 \, 3l$ and $4l$, the former mixing and interfering with $1s^2 2s^2 2p^5 \, 4l$ and $5l$ [12] and the latter mixing and interfering with $1s^2 2s^2 2p^5 6l$ and even higher levels.

For DC, there is a basic need for atomic data, not available at the time of the experiment. The exit channels are sodiumlike core excited states such as Ar^{7+}($1s^2 2s^2 2p^5 3ln'l'$)$^{2,4}L_J$ with $n'=4$ and 5. The calculations of the atomic data are performed in the LSJ coupling scheme, which is suitable to take into account correlation and relativistic effects [20].

We study the Ar^{9+}-He charge-transfer collision at a kinetic energy of 2.25 keV/amu. Above the ground state of the fluorinelike projectile $1s^2 2s^2 2p^5 \, ^2P^o_{3/2}$, there is a metastable one, $1s^2 2s^2 2p^5 \, ^2P^o_{1/2}$ (2.2 eV higher). It may decay to the ground state by a magnetic dipole transition in the visible range. We calculated the wavelength and transition probability to be ~ 5500 Å and $A_{ij} \sim 1.3 \times 10^2$ s^{-1}. An important feature is underlined: the excitation energy of the ground state to reach $1s^2 2s 2p^6 \, ^2S_{1/2}$ is of the order of 77.1 eV; the radiative transition probability back to the ground state is $A_{ij} \approx 4.42 \times 10^{10}$ s^{-1}.
SC will give

$$\text{Ar}^{9+} + \text{He} \rightarrow \text{Ar}^{8+}(1s^2 2s^2 2p^5 nl)^{1,3}L_J + \text{He}^+, \quad (1)$$

---
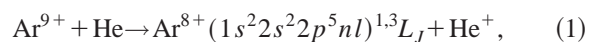
*Author to whom correspondence should be addressed.
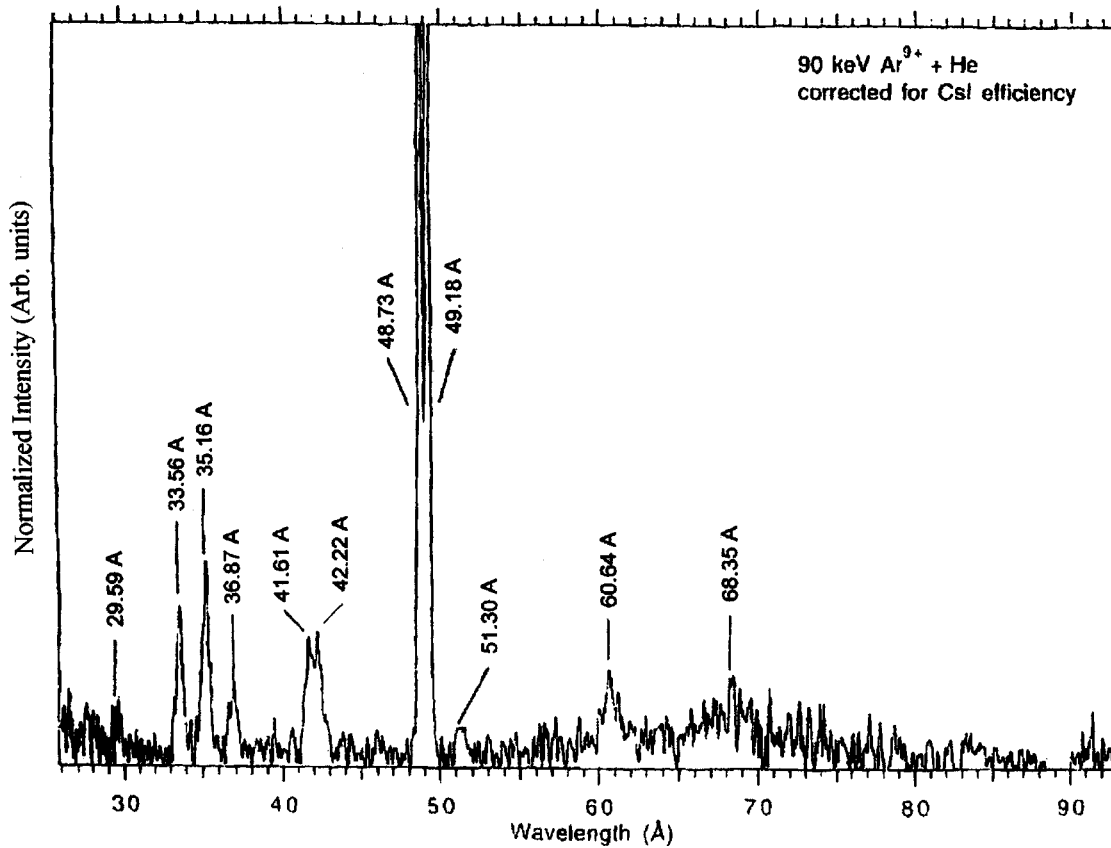
FIG. 1. XUV-VUV spectrum in the wavelength window 25–90 Å from the decay following the collision Eq. (1). Normalized intensity (arbitrary units) versus wavelength (Å).

where the available scaling rules predict that n will share among $n=4$ and 5 while $l=0,1$ [18] are expected to be most populated. This is slightly different from the scaling for l suggested in [19] where the collision target was not specified. However, the value from [19] retaining and considering the specifics of our case, introducing in l [19] the cross section determined from our experimental scaling [21] predicts that the most probably populated angular momentum will be $l=2$. It is, however, stated that the l distribution is not expected to be statistical, confirming some of our previous observations [22].

Double-electron capture will populate sodiumlike core excited states:

$$Ar^{9+} + He \rightarrow Ar^{7+}(1s^2 2s^2 2p^5 nl, n'l')^{2,4}L_J + He^{++}. \quad (2)$$
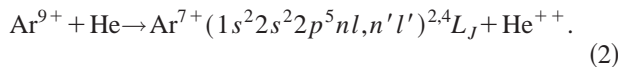
According to the scaling rules, the most populated levels are expected to be $(1s^2 2s^2 2p^5 3l \ 4l'$ and $5l')$.

In Sec. II, we present the experiments, the experimental techniques used, and the experimental results. In Sec. III, the theoretical calculations for the analysis and identification of the optical (SC) and Auger (DC) spectra are presented and discussed. Section IV gives an extensive analysis and the proposed identifications in the core excited neonlike and sodiumlike argon ion. Section IV considers also the collision features and cross sections. We insist on the fact that the charge-transfer collision is in fact a strong interaction occur-

ring at small internuclear distances, mixing the populated states. The cross sections are estimated.

II. EXPERIMENTAL DEVICE, METHODS, AND RESULTS

The Ar^{9+}-He collision system has been studied with different experimental techniques. On the one hand, x-ray and vacuum ultraviolet (XUV and VUV) photon spectroscopy was applied to the observation of the decay following SO and DC at an energy of 90 keV. For the sake of completeness, the analysis of the DC was performed using an Auger spectrum taken in the same experimental conditions as the VUV spectrum and that was not fully analyzed and interpreted [23].

The optical spectrum resulting from the process Eq. (1) is compared with the optical spectrum resulting from

$$Ar^{8+} + He \rightarrow Ar^{7+}(1s^2 2s^2 2p^6 nl)^2 L_J + He^+ \quad (3)$$
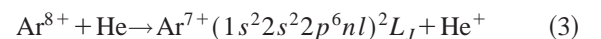
in the wavelength interval 90–160 Å for calibration purposes. Comparison of the spectra from the processes Eq. (1) and Eq. (3) in this wavelength interval shows that no lines from the normal Na-like spectrum [Eq. (3)] are seen in the Ne-like spectrum of the system Eq. (1).

The Auger spectrum [Eq. (2)] is compared with the one resulting from SC and DC:
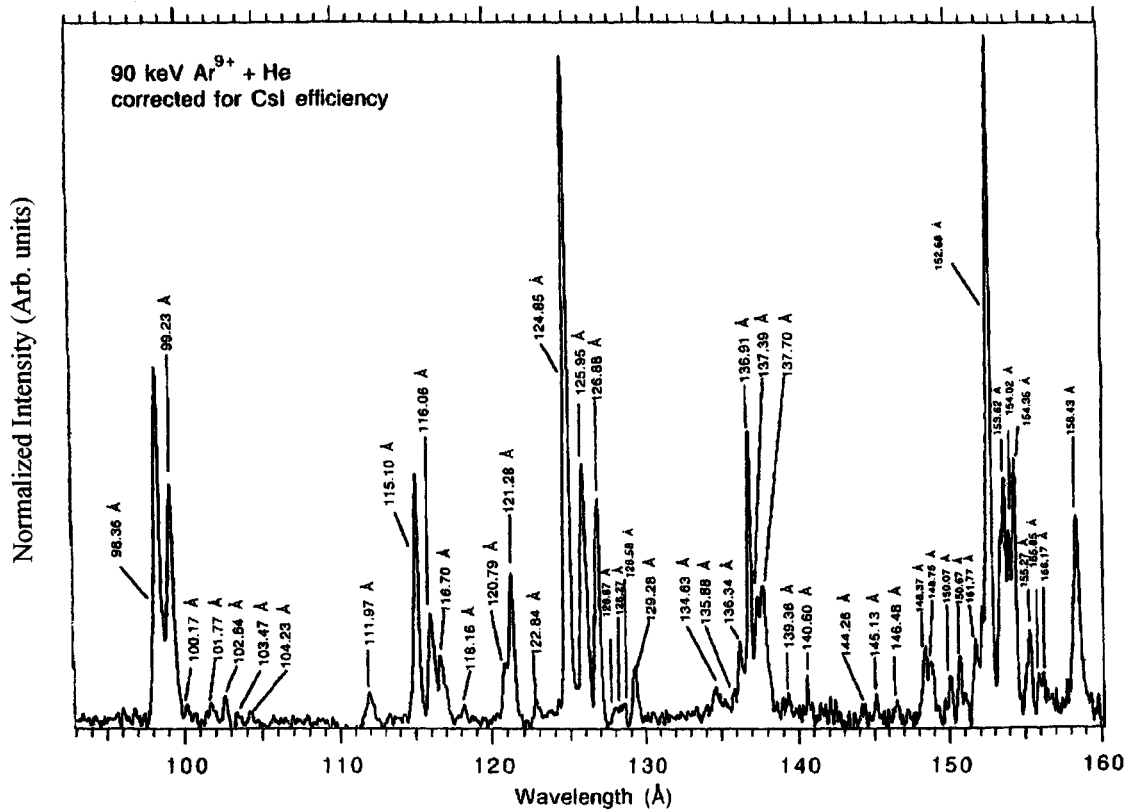
FIG. 2. XUV-VUV spectrum in the wavelength window 90–160 Å from the decay following the collision Eq. (1). For units, see Fig. 1.

$$Ar^{8+}(1s^2 2s^2 2p^5 3s)^3 P_{0,2} + He$$

$$\rightarrow Ar^{7+}(1s^2 2s^2 2p^5 3l n' l')^{2,4} L_J. \qquad (4)$$
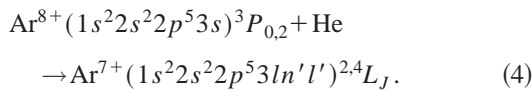
This comparison gives an energy calibration for the Auger electrons. It underlines the fact that the states populated in

the collision Eq. (2) share between doublets and quartets and have a single available continuum to decay to.

The experimental device was described previously and is rapidly presented. It basically uses an electron cyclotron resonance (ECR) ion source that delivers multiply charged ion beams. Once accelerated, a bending magnet analyzes the
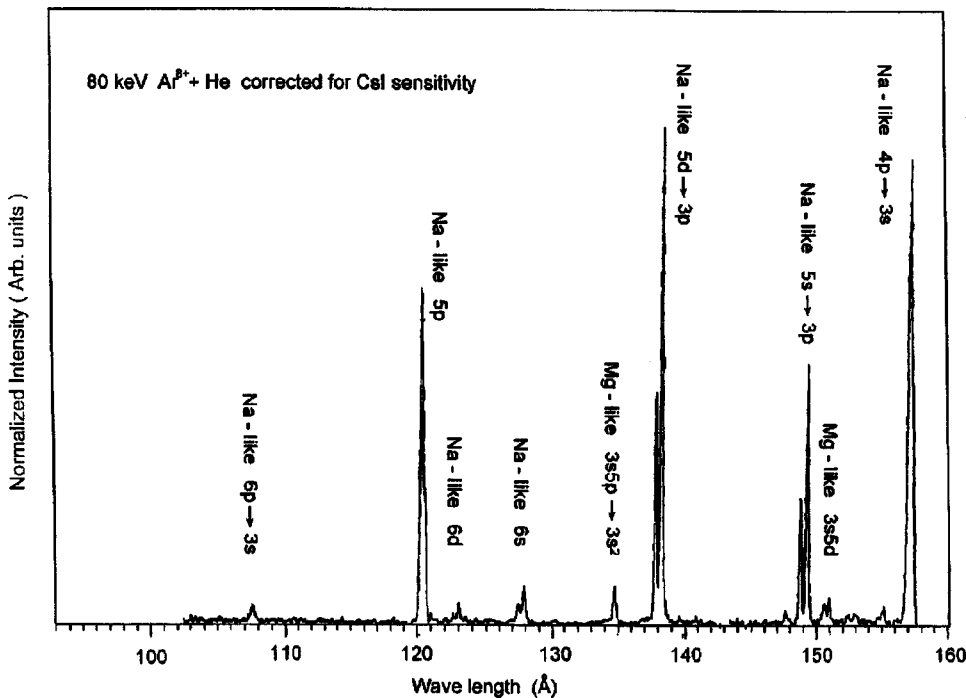
FIG. 3. XUV-VUV spectrum in the wavelength window 90–160 Å from the decay following the collision Eq. (3). For units, see Fig. 1.
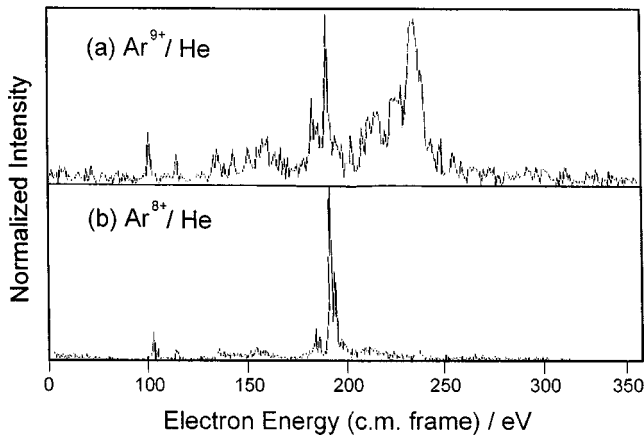
FIG. 4. (a) Auger spectrum in the emitter frame energy window 0–350 eV and following process Eq. (2). Intensity (arbitrary units) versus energy (eV) of the electron in the emitter frame. (b) Auger spectrum in the emitter frame energy window 0–300 eV following process Eq. (4). Intensity (arbitrary units) versus energy (eV) of the electron in the emitter frame.

ion beam and selects the needed specific mass-to-charge ratio. This selected beam is passed into a differentially pumped collision cell. The pressure of He is adjusted at a typical pressure of order $(3-4) \times 10^{-3}$ Pa and monitored using a Baratron.

A. XUV-VUV spectroscopy

The argon-ion beam delivered by the ECR ion source at the University of Nevada, Reno, facility is charge and mass analyzed to obtain a pure Ar^{9+} beam. The typical ion current is of the order of 1 μA at 90 keV (ion velocity $v \approx 0.29$ a.u.). The grazing-incidence spectrometer faces directly into the collision cell at 90° to the incident ion beam [7]. The wavelength windows were set to observe the intervals 25–90 and 90–160 Å. In Fig. 1 we show the part 25–90 Å where the transitions $2p^53s\ ^1P_1^o$ and $^3P_1^o$ to $2p^6\ ^1S_0$ at 48.73 and 49.18 Å, respectively, can be seen. A limited number of the transitions appearing in this figure were still not known before our identification. In Fig. 2, the spectrum shows some totally unknown transitions. For the purpose of comparison and wavelength calibration the spectrum of the decay following reaction (3) is presented (it is the sodiumlike spectrum of Ar^{7+}) in the interval 90–160 Å in Fig. 3. Weak-intensity lines are seen and are interpreted as resulting from DC by Ar^{8+}. The ion energy was 80 keV, the other experimental conditions being the same as for Ar^{9+}(90 keV). In Sec. III, the calculated data for identification of the lines are presented.

B. Auger spectroscopy

As shown in earlier discussions [23], for the sake of completeness, we show here an Auger spectrum [Fig. 4(a)]; it was taken in the same experimental conditions as the XUV-VUV spectra of Figs. 1 and 2: Ar^{9+} ion energy 90 keV. This spectrum, as appears hereafter, was not fully analyzed and attributions were incomplete. A good reference spectrum

to interpret and make attributions is shown in Fig. 4(b). It represents the Auger spectrum obtained in the stabilization following process Eq. (4). This spectrum was fully analyzed and shown to be the consequence of SC and DC [24]. It is important since it gives an energy reference; some lines are common to both Auger spectra.

III. THEORETICAL CALCULATIONS

As explained above we need data for the analysis of SC and DC by the fluorinelike argon projectile $1s^22s^22p^5\ ^2P_{3/2}^o$ as well as for line identifications. The SC ends in the formation of core excited neonlike argon while the DC ends in core excited sodiumlike argon according to Eqs. (1) and (2).

To perform the calculations of the needed atomic data, we use the SUPERSTRUCTURE code developed by Eissner, Jones, and Nussbaumer [25], which provides energy levels, wavelengths, and spontaneous radiative decay rates. Wave functions are determined by diagonalization of the nonrelativistic Hamiltonian using orbitals calculated in a scaled Thomas-Fermi-Dirac-Amaldi potential, different for each angular momentum l for the one-electron orbitals. These potentials depend closely on the configurations that are introduced. Spin-orbit and relativistic corrections (mass, Darwin, and one-body operators) are introduced according to the Breit-Pauli approach and the results are obtained in the intermediate coupling LSJ. The multiconfiguration basis set we used contains all the configurations $1s^22s^22p^6$, $1s^22s^22p^5nl$ with $n=3,4,5$ and $0 \leq l \leq n-1$, and $1s^22s2p^6nl$ with $n=3$ and 4 and $0 \leq l \leq n-1$. This corresponds to 23 configurations, 77 terms, and 141 levels. The scaling parameters are obtained by the minimization procedure of the energy sum of all terms belonging to the following configurations: $1s^22s^22p^6$, $1s^22s^22p^5nl$ with $n=3$ and $0 \leq l \leq n-1$. The values obtained are 1.2010 for λ_s, 1.1304 for λ_p, and 1.0951 for $\lambda_d = \lambda_f$. These scaling parameters are used in the multiconfiguration basis set to calculate energy levels, wavelengths, and spontaneous radiative decay rates in the intermediate coupling LSJ.

In Table I the level energies relative to the ground state are displayed. To give a global view of them, Grotrian diagrams of singlet and triplet levels are shown separately in Figs. 5 and 6 (their relative positions are better appreciated than if all the levels were represented in a single diagram). One should note that the levels $1s^22s2p^63s$ and $1s^22s2p^63p$ interfere strongly with $1s^22s^22p^54l$ levels while $1s^22s2p^63d$ levels interfere with $1s^22s^22p^55l$ levels. The levels with open core, from $1s^22s2p^64s\ ^3S_1$ up to $1s^22s2p^64p\ ^1P_2$, will interfere with highly excited levels above $5f$. As seen in Table I, all the levels from $1s^22s2p^64s\ ^3S_1$ up to $1s^22s2p^64p\ ^1P_2$ are under the ionization limit while from $1s^22s2p^64d\ ^3D_1$ all the levels are above it.

To ease the identification of the lines and attributions, J. F. Wyart performed an extended calculation using the code developed by Cowan [26]. This is intended to facilitate the identification on the basis of a comparative approach: in the actual experimental situation l sharing is not statistical. This differs notably from the plasma case in thermal equilibrium

TABLE I. Level energies relative to the ground state (in Ry) for neonlike argon. Levels with open subshells $1s^22s2p^6nl$ are shown. From $1s^22s2p^64d\,^3D_1$ on, they are above the ionization limit.

Level	Energy	Level	Energy	Level	Energy
$1s^22s^22p^6\,^1S_0$	0.000 000	$1s^22s^22p^53d\,^3D_2$	21.593 448	$1s^22s^22p^54d\,^3P_1$	25.527 822
$1s^22s^22p^53s\,^3P_2$	18.287 284	$1s^22s^22p^53d\,^1F_3$	21.594 977	$1s^22s^22p^54d\,^3F_4$	25.530 719
$1s^22s^22p^53s\,^3P_1$	18.354 398	$1s^22s^22p^53d\,^1P_1$	21.856 992	$1s^22s^22p^54d\,^3F_3$	25.544 292
$1s^22s^22p^53s\,^3P_0$	18.487 838	$1s^22s2p^63s\,^3S_1$	24.065 722	$1s^22s^22p^54d\,^3P_2$	25.544 545
$1s^22s^22p^53s\,^1P_1$	18.555 304	$1s^22s2p^63s\,^1S_0$	24.358 687	$1s^22s^22p^54d\,^1D_2$	25.565 453
$1s^22s^22p^53p\,^3S_1$	19.405 871	$1s^22s^22p^54s\,^3P_2$	24.403 888	$1s^22s^22p^54d\,^3D_3$	25.576 704
$1s^22s^22p^53p\,^3D_3$	19.599 342	$1s^22s^22p^54s\,^1P_1$	24.436 031	$1s^22s^22p^54d\,^3d_1$	25.656 902
$1s^22s^22p^53p\,^3D_2$	19.606 574	$1s^22s^22p^54s\,^3P_0$	24.601 706	$1s^22s^22p^54f\,^3D_1$	25.717 954
$1s^22s^22p^53p\,^1P_1$	19.665 513	$1s^22s^22p^54s\,^3P_1$	24.624 277	$1s^22s^22p^54f\,^3D_2$	25.723 332
$1s^22s^22p^53p\,^3P_2$	19.713 075	$1s^22s^22p^54p\,^3S_1$	24.894 943	$1s^22s^22p^54f\,^3D_3$	25.742 464
$1s^22s^22p^53p\,^3D_1$	19.806 132	$1s^22s^22p^54p\,^3D_3$	24.910 862	$1s^22s^22p^54f\,^3F_2$	25.742 943
$1s^22s^22p^53p\,^3P_0$	19.827 084	$1s^22s^22p^54p\,^3D_2$	24.915 026	$1s^22s^22p^54f\,^3G_5$	25.744 721
$1s^22s^22p^53p\,^1D_2$	19.865 574	$1s^22s^22p^54p\,^1P_1$	24.940 664	$1s^22s^22p^54f\,^1G_4$	25.744 925
$1s^22s^22p^53p\,^3P_1$	19.871 242	$1s^22s^22p^54p\,^3P_2$	24.953 916	$1s^22s^22p^54f\,^1D_2$	25.748 043
$1s^22s^22p^53p\,^1S_0$	20.711 934	$1s^22s^22p^54p\,^3P_0$	25.064 817	$1s^22s^22p^54d\,^3D_2$	25.752 052
$1s^22s^22p^53d\,^3P_0$	21.221 581	$1s^22s^22p^54p\,^3D_1$	25.108 309	$1s^22s^22p^54d\,^3D_1$	25.758 022
$1s^22s^22p^53d\,^3P_1$	21.244 139	$1s^22s^22p^54p\,^1D_2$	25.133 591	$1s^22s^22p^54f\,^1F_3$	25.760 025
$1s^22s^22p^53d\,^3P_2$	21.289 596	$1s^22s^22p^54p\,^3P_1$	25.135 646	$1s^22s^22p^54f\,^3F_4$	25.761 143
$1s^22s^22p^53d\,^3F_4$	21.318 803	$1s^22s2p^63p\,^3P_0$	25.378 524	$1s^22s^22p^54d\,^1P_1$	25.873 575
$1s^22s^22p^53d\,^3F_3$	21.346 179	$1s^22s2p^63p\,^3P_1$	25.387 956	$1s^22s^22p^54f\,^3F_3$	25.942 637
$1s^22s^22p^53d\,^3F_2$	21.397 450	$1s^22s2p^63p\,^3P_2$	25.412 334	$1s^22s^22p^54f\,^3F_2$	25.946 222
$1s^22s^22p^53d\,^3D_3$	21.435 025	$1s^22s^22p^54p\,^1S_0$	25.457 967	$1s^22s^22p^54f\,^3G_3$	25.950 974
$1s^22s^22p^53d\,^3D_2$	21.535 941	$1s^22s2p^63p\,^1P_1$	25.481 855	$1s^22s^22p^54f\,^3G_4$	25.952 544
$1s^22s^22p^53d\,^1D_2$	21.565 880	$1s^22s^22p^54d\,^3P_0$	25.515 104	$1s^22s^22p^55s\,^3P_2$	26.929 633
$1s^22s^22p^55s\,^1P_1$	26.942 983	$1s^22s^22p^55p\,^1S_0$	27.543 466	$1s^22s2p^64d\,^3D_2$	31.268 750
$1s^22s2p^63d\,^3D_1$	27.069 685	$1s^22s^22p^55f\,^3G_5$	27.572 135	$1s^22s2p^64d\,^3D_3$	31.270 499
$1s^22s2p^63d\,^3D_2$	27.069 690	$1s^22s^22p^55f\,^1G_4$	27.572 477	$1s^22s2p^64d\,^1D_2$	31.333 040
$1s^22s2p^63d\,^3D_3$	27.070 335	$1s^22s^22p^55f\,^1F_3$	27.580 119	$1s^22s2p^64f\,^3F_2$	31.471 896
$1s^22s^22p^55s\,^3P_0$	27.130 288	$1s^22s^22p^55f\,^3F_4$	27.580 767	$1s^22s2p^64f\,^3F_3$	31.472 208
$1s^22s^22p^55s\,^3P_1$	27.137 579	$1s^22s^22p^55f\,^3F_2$	27.587 927	$1s^22s2p^64f\,^3F_4$	31.472 811
$1s^22s^22p^55p\,^3S_1$	27.149 484	$1s^22s^22p^55f\,^3F_3$	27.588 020	$1s^22s2p^64f\,^1F_4$	31.475 128
$1s^22s^22p^55p\,^1D_2$	27.167 774	$1s^22s^22p^55f\,^3D_1$	27.592 831	$1s^22s2p^65s\,^3S_1$	32.659 169
$1s^22s^22p^55p\,^1P_1$	27.186 079	$1s^22s^22p^55f\,^3D_2$	27.594 231	$1s^22s2p^65s\,^1S_0$	32.717 104
$1s^22s^22p^55p\,^3P_2$	27.186 621	$1s^22s^22p^55d\,^3F_2$	27.668 592	$1s^22s2p^65p\,^3P_0$	32.897 772
$1s^22s^22p^55p\,^3D_3$	27.188 071	$1s^22s^22p^55d\,^3D_2$	27.671 247	$1s^22s2p^65p\,^3P_1$	32.899 608
$1s^22s2p^63d\,^1D_2$	27.240 771	$1s^22s^22p^55d\,^1F_3$	27.676 586	$1s^22s2p^65p\,^3P_2$	32.905 154
$1s^22s^22p^55p\,^3P_0$	27.286 527	$1s^22s^22p^55d\,^1P_1$	27.729 998	$1s^22s2p^65p\,^1P_1$	32.900 754
$1s^22s^22p^55p\,^3D_1$	27.371 366	$1s^22s^22p^55f\,^3G_3$	27.775 773	$1s^22s2p^65d\,^3D_1$	33.190 967
$1s^22s^22p^55p\,^3P_1$	27.377 081	$1s^22s^22p^55f\,^3G_4$	27.776 749	$1s^22s2p^65d\,^3D_2$	33.191 553
$1s^22s^22p^55p\,^3D_2$	27.386 038	$1s^22s^22p^55f\,^1D_2$	27.785 977	$1s^22s2p^65d\,^3D_3$	33.192 479
$1s^22s^22p^55d\,^3P_0$	27.446 991	$1s^22s^22p^55f\,^3D_3$	27.786 237	$1s^22s2p^65d\,^1D_2$	33.226 043
$1s^22s^22p^55d\,^3P_1$	27.454 588	$1s^22s2p^64s\,^3S_1$	30.162 553	$1s^22s2p^65f\,^3F_2$	33.296 112
$1s^22s^22p^55d\,^3F_4$	27.462 675	$1s^22s2p^64s\,^1S_0$	30.272 112	$1s^22s2p^65f\,^3F_3$	33.296 288
$1s^22s^22p^55d\,^3P_2$	27.466 094	$1s^22s2p^64p\,^3P_0$	30.653 591	$1s^22s2p^65f\,^3F_4$	33.296 593
$1s^22s^22p^55d\,^3F_3$	27.470 100	$1s^22s2p^64p\,^3P_1$	30.657 075	$1s^22s2p^65f\,^1F_3$	33.298 392
$1s^22s^22p^55d\,^1D_2$	27.480 644	$1s^22s2p^64p\,^3P_2$	30.667 402		
$1s^22s^22p^55d\,^3D_3$	27.486 001	$1s^22s2p^64p\,^1P_1$	30.696 965		
$1s^22s^22p^55d\,^3D_1$	27.539 358	$1s^22s2p^64d\,^3D_1$	31.267 645		
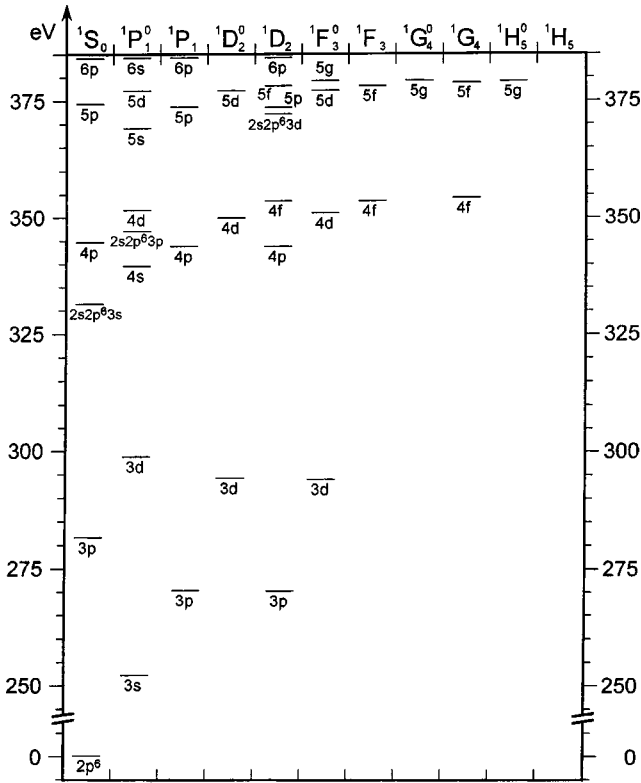
FIG. 5. Grotrian diagram of the neonlike argon singlet levels. Energy scale in eV from ground state

FIG. 6. Grotrian diagram of the neonlike argon triplet levels. Energy scale as in Fig. 5.

where l sharing is statistical. The observations are frequently limited to the transitions from the lowest-lying levels above the ground states. Some known transitions are also used for calibration and comparison purposes [13(b)].

In Tables II and III we present the calculated wavelengths of the allowed transitions in the 30–50 and 95–160 Å ranges, respectively, and the suggested identifications of the experimentally observed lines.

To calculate the atomic data needed for the analysis of the Auger spectrum resulting from DC by fluorinelike argon, we used the multiconfiguration basis set $1s^2 2s^2 2p^6 nl$ with n

$=3$ and $0 \leq l \leq n-1$, $1s^2 2s^2 2p^5 nl, n'l'$ with $n=3$ and $l=1,2$ and $n'=4,5$ and $0 \leq l \leq n-1$. This choice is dictated by the fact that in previous papers the doubly excited levels for $3s3l'$, $3s4l'$, and $3s5l'$ were determined [6,7]. This choice leads to 16 configurations, 318 terms in *LS* coupling and 778 levels in *LSJ* coupling. The scaling parameters $\lambda_s = 1.0795$, $\lambda_p = 1.0065$, and $\lambda_d = \lambda_f = 0.9124$ used are obtained by the minimization of the energy sum of all terms belonging to the following configurations. $1s^2 2s^2 2p^6 nl$ with $n=3$ and $0 \leq l \leq n-1$. To ease the analysis and identification, we determined the energy range of the $(4l, n'l')$

TABLE II. Wavelengths of the transitions in the range 29–50 Å. Column 1 transitions to the ground level. Column 2: theoretical wavelength for the decays to the ground state from this calculation, $\lambda_{\text{th Cornille}}$. Column 3: experimental wavelengths (this paper) $\lambda_{\text{obs Bliman}}$. Column 4: experimental wavelengths of [13(b)], $\lambda_{\text{obs Faucett}}$.

Transition	$\lambda_{\text{th Cornille}}$ (Å)	$\lambda_{\text{obs Bliman}}$ (Å)	$\lambda_{\text{obs Faucett}}$ (Å)
$1s^2 2s 2p^6 4p\ {}^1P_1 - 1s^2 2s^2 2p^6\ {}^1S_0$	29.6859	29.59	
$1s^2 2s^2 2p^5 5s\ {}^1P_1 - 1s^2 2s^2 2p^6\ {}^1S_0$	33.8221	33.56	
$1s^2 2s^2 2p^5 4d\ {}^1P_1 - 1s^2 2s^2 2p^6\ {}^1S_0$	35.2200	35.16	35.024
$1s^2 2s^2 2p^5 4d\ {}^3D_1 - 1s^2 2s^2 2p^6\ {}^1S_0$	35.5174	35.260	
$1s^2 2s^2 2p^5 4d\ {}^3P_1 - 1s^2 2s^2 2p^6\ {}^1S_0$	35.6970	35.422	
$1s^2 2s^2 2p^5 4s\ {}^3P_1 - 1s^2 2s^2 2p^6\ {}^1S_0$	37.0069	36.87	36.983
$1s^2 2s^2 2p^5 3d\ {}^1P_1 - 1s^2 2s^2 2p^6\ {}^1S_0$	41.6924	41.61	41.4760
$1s^2 2s^2 2p^5 3d\ {}^3D_1 - 1s^2 2s^2 2p^6\ {}^1S_0$	42.3138	42.22	42.0010
$1s^2 2s^2 2p^5 3d\ {}^3P_1 - 1s^2 2s^2 2p^6\ {}^1S_0$	42.8950		42.5290
$1s^2 2s^2 2p^5 3s\ {}^1P_1 - 1s^2 2s^2 2p^6\ {}^1S_0$	49.1109	48.73	48.7390
$1s^2 2s^2 2p^5 3s\ {}^3P_1 - 1s^2 2s^2 2p^6\ {}^1S_0$	49.6484	49.18	49.1850

TABLE III. Theoretical and observed wavelengths in the 95–160 (Å) range. Column 1: transitions. Column 2: theoretical wavelength (superstructure theory). Column 3: experimental observations (present values as identified). Column 4: Calculated values [Fawcett *et al.* [13(b)]]. Column 5: observed wavelengths [13(b)].

Transition	$\lambda_{\text{th Cornille}}$ (Å)	$\lambda_{\text{obs Bliman}}$ (Å)	$\lambda_{\text{th Fawcett}}$ (Å)	$\lambda_{\text{obs Fawcett}}$ (Å)
$1s^22s^22p^55p\ ^1S_0-1s^22s^22p^53s\ ^1P_1$	101.3853	101.17		
$1s^22s^22p^55p\ ^3d_2-1s^22s^22p^53s\ ^1P_1$	103.1927	103.47		
$1s^22s^22p^55p\ ^3D_1-1s^22s^22p^53s\ ^1P_1$	103.3644	104.23		
$1s^22s^22p^55d\ ^3P_1-1s^22s^22p^53p\ ^3S_1$	113.2189			
$1s^22s^22p^55d\ ^3P_0-1s^22s^22p^53p\ ^3S_1$	113.3259			
$1s^22s^22p^55d\ ^3F_3-1s^22s^22p^53p\ ^3D_2$	115.8853			
$1s^22s^22p^55d\ ^3F_4-1s^22s^22p^53p\ ^3D_3$	115.8882	115.10	114.91	115.197
$1s^22s^22p^55d\ ^1F_3-1s^22s^22p^53p\ ^1D_2$	116.6644	116.06	114.92	115.197b
$1s^22s^22p^55s\ ^3P_0-1s^22s^22p^53p\ ^3D_1$	124.4194	124.85	123.28	123.556
$1s^22s^22p^55s\ ^3P_1-1s^22s^22p^53p\ ^1D_2$	125.3117	125.95		
$1s^22s^22p^54p\ ^3D_3-1s^22s^22p^53s\ ^3P_2$	137.5793	136.91	136.52	136.164
$1s^22s^22p^55f\ ^3D_3-1s^22s^22p^53d\ ^3P_2$	144.6818	144.26	144.03	143.600
$1s^22s^22p^55f\ ^3G_5-1s^22s^22p^53d\ ^3F_4$	145.7251	145.13	144.48	144.512
$1s^22s^22p^54d\ ^3P_2-1s^22s^22p^53p\ ^3S_1$	148.4469	148.37	148.70	147.949
$1s^22s^22p^54d\ ^3P_1-1s^22s^22p^53p\ ^3S_1$	148.8524	148.75	149.15	148.390
$1s^22s^22p^54d\ ^3D_2-1s^22s^22p^53p\ ^3D_2$	150.8976	150.67	151.57	152.072
$1s^22s^22p^54d\ ^3F_4-1s^22s^22p^53p\ ^3D_3$	153.6350	152.68	152.18	152.692
$1s^22s^22p^54d\ ^3D_3-1s^22s^22p^53p\ ^3P_2$	154.4101	154.35	153.82	154.445
$1s^22s^22p^54d\ ^3P_2-1s^22s^22p^53p\ ^3P_2$	156.2671	155.27		
$1s^22s2p^63d\ ^3D_3-1s^22s^22p^53d\ ^3F_4$	158.4390	158.43		

FIG. 7. Energies of the different Auger series, in the emitter frame (eV), as calculated. The energies in the emitter frame are given assuming that all the series decay to the $2p^6\ ^1S_0$ continuum. The dashed parts of the series above 252 eV are in fact expected to decay to the $2p^53l$ continua.

series with $0 \leq l \leq n-1$ and n' from 4 to the series limit. The $4l^2$ terms were calculated and are given in [22]. The limit of each series is deduced from its energy position relative to $2p^53l$ (Fig. 8 below). This is summarized in Fig. 7, where the different Auger series energies are given in the emitter frame in eV under the assumption that they all decay to the $1s^22s^22p^6 \ {}^1S_0$ continuum. From the comparison with the Auger spectra [Figs. 4(a) and 4(b)], no transition seems to be attributable to the decay of the $(4l, n'l')$ series. This is discussed hereafter in Sec. IV. In Table IV are given the Auger-electron energies (in the emitter frame) relative to the continuum to which they decay ($1s^22s^22p^6 \ {}^1S_0$) since it is seen that the spectrum shows a clear energy limit around 250 eV. This is the limit of the series $1s^22s^22p^63snl$. It is now possible to make some tentative attributions and identifications and discuss the collision aspects.

IV. COLLISION FEATURES AND IDENTIFICATIONS

To ease the discussion of the collision features and the identifications in the XUV-VUV and Auger spectra, we start by giving the overall level diagram showing the relative energy positions of the entrance and exit channels (Fig. 8). A rapid survey of the right column shows that all $(4l, nl')$ should decay to the nearest available continua $1s^22s^22p^53l \ {}^{1,3}L$. This is from the analysis in [23].

A. Collision features

The collision features can be understood by considering different aspects. In terms of classical Landau-Zener theories [17,27–30] the SC process would take place at an internuclear distance of the order of 8 a.u. The second electron would be "molecularized" at roughly 3 a.u. The SC cross section in these conditions would be of order 5×10^{-15} cm^2. This value can be compared with that deduced from the experimental scaling rule [21], 2.5×10^{-15} cm^2 ($\pm 20\%$). Other cross sections for this system were taken at smaller energies than ours [31]. In their ion energy range from 4.5 eV to 9 keV, the SC cross section decreases smoothly from 9.4×10^{-15} down to 5×10^{-15} cm^2. It can be estimated that this trend will be observed with increasing energies until the cross section reaches a plateau as frequently observed, and the SC cross section at 90 keV will stabilize around 3×10^{-15} cm^2. The DC cross sections of [31] (around 2×10^{-16} cm^2) are nearly constant within the energy range 4.5 eV–9 keV. It has been calculated with the classical trajectory Monte Carlo calculation (CTMC) approach that in the low-energy collision region an ion colliding with a H target can capture a target electron in a totally predictable manner. The corresponding cross section has a plateau in the low-energy collision region E_c that can slightly increase for energies lower than 0.1 keV/amu. On the basis of previous calculations for the $p^+ + H$ collision given by Olson and Salop [32], an empirical formula was constructed by Janev [33] illustrating the aforementioned plateau formation. A number of recent four- and five-body CTMC's [34] have shown that the value of this plateau can be scaled for various atomic and molecular targets. It is not
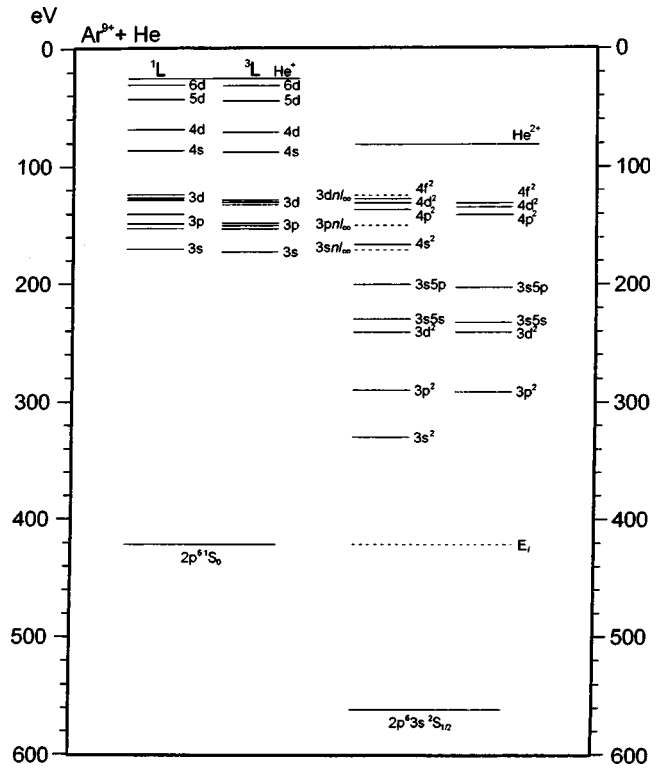
FIG. 8. Overall level diagram for the analysis of the collisions Ar^{9+}+He showing in column 1 (left) the entrance channel Ar$^{9+}(1s^22s^22p^5)^2P_J^o$; column 2 (center) the SC exit channel (upper part) and particularly the levels $1s^22s^22p^5$ 4l and 5l, column 3 (right) the sodiumlike core excited levels $1s^22s^22p^5 \ (3ln'l')$ and the extent of the $(4ln'l')$ level series.

sensitive to the projectile constitution. At higher energies, from around 20 keV/amu, the capture- and ionization-cross-section curve slopes are strongly dependent on the projectile constitution. Using this scaling, we are able to foresee for the collision Ar^{9+}+He a plateau lying between 1×10^{-15} and 10×10^{-15} cm^2 and slightly increasing for energies lower than $E_c < 1$ keV. Another group [35] working with Ar^{q+} ions ($14 \geq q \geq 8$) at an energy of $2.3q$ keV found for SC a cross section of the order of 3×10^{-15} cm^2 and for total DC (radiation and autoionization stabilized) a cross section of order 3×10^{-16} cm^2. In our experimental conditions, the DC cross section would be near 4×10^{-16} cm^2. Of course, some uncertainty in that cross section comes from the autoionization Auger decay that feeds the SC exit channel.

A further step to ease the analysis of this collision system can now be performed; it consists in considering the time-ordering sequence for the processes taking place from the entrance to the exit of the collision. The overall collision duration can be roughly estimated; it is of the order of $t_{\text{collision}} \approx \sqrt{\sigma}/v$, where σ is the capture cross section and v the projectile velocity. With the actual values, this time is of order 8×10^{-16} s. From the very moment the first target electron is "molecularized" until the transfer of the second takes place the elapsed time can be estimated to be $t_{1 \rightarrow 2} \approx \Delta R/v$, where ΔR is the distance between potential curve crossings. In our conditions, this elapsed time is of order 3.8×10^{-16} s. The other relevant characteristic times are the

lifetimes of the levels populated in SC and DC. For the Ne-like argon levels, typical lifetimes are of the order of 10^{-12} s, whereas the Na-like core excited argon levels are not expected to survive for more than 10^{-13}–10^{-14} s. An important time delay is the time that elapses between two successive collisions; since we meet the single-collision condition, this mean time is $t_{\mathrm{mean}}=(N_n\sigma v)^{-1}$, where N_n is the neutral number gas density in the collision chamber, σ the capture cross section, and v the projectile velocity; in the actual conditions it is of the order of 8.5×10^{-6} s. This means that the distance the ion flies between two successive collisions is nearly 5×10^2 cm. Finally, the last relevant time in this sequence is the time that has elapsed from the beginning of the collision until the optical and Auger spectroscopies begin: $t_{\mathrm{observation}}$. To summarize, the full sequence is

$$t_{1\to2}<t_{\mathrm{collision}}<t_{\mathrm{Auger}}<t_{\mathrm{radiation}}$$

$$<t_{\mathrm{observation}}<t_{\mathrm{mean}}.$$

Another aspect is considered to answer the question: Is there any experimental evidence of correlated double-electron capture? On the basis of the identifications in the Auger spectrum, all populated states have different n values. No Auger electrons seem to have their origin in $n=n'=4$. The Auger spectrum shows that the center of the DC window is on $n=3$, $n'=5$, and the limit is at 250 eV, the limit of the $2p^53snl$ series. This supports the representation of a two-step process in DC.

B. Optical spectrum identifications

It should be noted that one attempt to this collision pair optically observe has been performed in the visible range (2500–8000 Å) [27]. The collision energy was 180 keV. It aimed at observing doubly excited levels of Ar^{7+}, this ion resulting from DC by Ar^{9+}. These Rydberg levels are high above the most populated levels (those we discuss in the present paper), typically $2p^53s8k\to2p^53s7i$ at 2950 Å. But the most prominent transitions resulting from DC by Ar^{9+} in the XUV-VUV range were not observed.

The accuracy of the measured wavelengths is of the order of ±0.01 Å.

We begin with the wavelength interval 30–50 Å in which more was known previously. One notes the extremely high intensity of the transitions $3s$ $^{1,3}P_1^o$ back to the ground state. In funnel-type decay, most excited levels above $2p^53s$ $^{1,3}P_J^o$ and of the general form $2p^5nl$ $^{1,3}L_J$ (with $n\geqslant3$ and $L\neq1$) will cascade down to $3s$. The ns and nd $^{1,3}P_1^o$ levels will have a branch decaying to the ground level.

Given the resolution $\Delta\lambda/\lambda$ of our spectrometer of the order of 5×10^{-5}, it is not possible to fully separate each individual transition. In the spectrum of Fig. 1 (25–90 Å) the most intense transitions are recognized as the decay of $2p^53s$ $^{1,3}P_1^o$ to the ground state $2p^6$ $^1S_0$ at, respectively, 48.73 and 49.18 Å. The group around 41–42 Å is attributable to $2p^53d$ $^{1,3}P_1^o\to2p^6$. We could not separate the $3d$ $^3P_1^o\to2p^6$ transition (the long-wavelength side of the group of transitions at 42.22 Å shows a shoulder likely to be

it). The group in the region 35–37 Å can be attributed to the $2p^54s$ $^{1,3}P_1^o$ and $2p^54d$ decays to the ground state [15]. At 33.56 Å it could be suggested that the broad peak is the transition from $5s$ $^{1,3}P_1^o$ to the ground state. Finally, at 29.59 Å, we suggest the decay to the ground state from the open core level $1s^22s2p^64p$ $^1P_1^o$. This underlines unambiguously that, in SC, $n=4$ and 5 are predominantly populated. The low-intensity peak at 51.30 Å could be identified as due to the decay of $2p^53s^2$ $^2P_J^o$ to the ground state $2p^63s$ ^2S. The fluorescence yield of the upper levels is of the order of 20% [36] but they are cascade populated. Some low-intensity peaks remain unidentified. Table II gives the calculated wavelengths of transitions suggested for the identification of our experimental ones. We note that the set of identified transitions is more complete than the one discussed by Fawcett *et al.* [13(b)]. In our case, the ion beam current is highly stable in time. The gaseous collision target pressure is low enough to satisfy the single-collision condition and is precisely regulated. With the detector of our spectrometer, single-pass recording of the spectrum was done.

In Table III, we give the transition identifications with comparisons to two different calculations and for the experimentally measured values with the observations of Fawcett *et al.* [13(b)] for the region 98–160 Å. The analysis and identifications of the spectrum in the region 98–160 Å raise many problems. We suggest here that this extended window be considered as small regions corresponding to the $n=5$ to 3 transitions: $5p\to3s$ (100–104 Å), $5d\to3p$ (112–121 Å), $5s\to3p$ (124–126 Å), and $5f\to3d$ (144–146 Å). Some intense $n=4$ to 3 transitions are intermingled with $n=5$ to 3: for example, $4p\to3s$ transitions in the interval 130–138 Å. The transitions $4d\to3p$ are seen in the interval 148–156 Å. A transition is identified as originating from an open core level, namely, $1s^22s2p^63d$ $^3D_3$. These identifications are guided by the use of the experimental scaling rule predictions, which are the most populated levels in SC: in the present case, $n=4$ and 5. Moreover, the largest gf factor, high values for the emission factor, and the largest possible branching ratios for the upper levels of the transitions and transition probabilities are the important guiding quantities. A transition intensity is usually proportional to geometric factors times the transition probability times the transition upper-level population [37]. In the present situation we observe two transitions from the capture levels of high intensities at 124.85 and 152.68 Å. Considering the transition probabilities for the upper levels, we can estimate the population of $5s$ to be of the order of a factor of 3 larger than that of $4d$.

The experimental method that Fawcett *et al.* [13(b)] used for recording their VUV spectrum was the observation of a pinch discharge; they needed 500 shots for sufficient exposure of the photographic plate. Comparing with Fawcett *et al.*'s identifications, we note that they have not done any observations below 112 Å, the spectral region where we identify $5p\to3s$ transitions. The global consistency of our identifications does not imply the consideration of possible $6f\to3d$ transitions but rather $5s\to3p$ around 125 Å, even though the energies of $6f$ levels were not calculated. Mention should be made that we cannot decide which of the two

TABLE IV. Theoretical Auger-electron energies relative to the ground state (in eV) for the stabilization following DC by the Ar^{9+} projectile.

Configuration	E_{th}
$1s^2 2s^2 2p^5 3s^2\ ^2P_{3/2}$	98.4077
$1s^2 2s^2 2p^5 3s^2\ ^2P_{1/2}$	100.7260
$1s^2 2s^2 2p^5 3s4f\ ^2G_{7/2}$	192.6900
$1s^2 2s^2 2p^5 3p4s\ ^4S_{3/2}$	196.4125
$1s^2 2s^2 2p^5 3p4s\ ^2D_{3/2}$	201.9370
$1s^2 2s^2 2p^5 3p4p\ ^4P_{1/2}$	202.2094
$1s^2 2s^2 2p^5 3p4p\ ^2P_{1/2}$	210.8483
$1s^2 2s^2 2p^5 3p4d\ ^4D_{1/2}$	211.6460
$1s^2 2s^2 2p^5 3p4d\ ^2S_{1/2}$	218.2041
$1s^2 2s^2 2p^5 3d4s\ ^4P_{1/2}$	222.9496
$1s^2 2s^2 2p^5 3d4s\ ^2F_{7/2}$	226.7807
$1s^2 2s^2 2p^5 3p5s\ ^4D_{7/2}$	228.5518
$1s^2 2s^2 2p^5 3p5s\ ^2D_{5/2}$	228.8589
$1s^2 2s^2 2p^5 3d4p\ ^2P_{1/2}$	229.5069
$1s^2 2s^2 2p^5 3d4p\ ^2P_{3/2}$	235.8936
$1s^2 2s^2 2p^5 3p5d\ ^4G_{11/2}$	235.9436
$1s^2 2s^2 2p^5 3p5d\ ^2P_{1/2}$	237.4900
$1s^2 2s^2 2p^5 3p4d\ ^2D_{3/2}$	237.6441
$1s^2 2s^2 2p^5 3p4d\ ^2P_{3/2}$	244.9162
$1s^2 2s^2 2p^5 3d4d\ ^2P_{1/2}$	248.3341

TABLE V. Auger lines for the stabilization following DC by Ar^{9+} in the energy range 100–200 eV (in the emitter frame). For the Auger lines in the energy range 200–250 eV, see text.

Electron energy (eV)	Normalized intensity	Tentative assignment
1.006×10^2	2.872×10	$1s^2 2s^2 2p^5 3s^2\ ^2P_{3/2}$
1.021×10^2	1.419×10	$1s^2 2s^2 2p^5 3s^2\ ^2P_{1/2}$
1.914×10^2	9.696×10	$1s^2 2s^2 2p^5 3s4f\ ^2G_{7/2}$
1.958×10^2	2.804×10	$1s^2 2s^2 2p^5 3p4s\ ^4S_{3/2}$
1.985×10^2	2.331×10	$1s^2 2s^2 2p^5 3p4s\ ^2D_{3/2}$
1.926×10^2	9.932×10	$1s^2 2s^2 2p^5 3s4f\ ^2G_{7/2}$
1.979×10^2	1.288×10	$1s^2 2s^2 2p^5 3p4s\ ^2D_{3/2}$

7). There do not seem to be lines attributable to the decay of any $4nl'$. They are all energetically located above the $3dnl$ series limit and they would not decay, if they had been populated in the DC process, to $2p^6\ ^1S_0$ as appears in Figs. 7 and 8. So, for the identifications, we are led to consider mostly the terms in the $3snl$, $3pn'l'$, and $3dn''l''$ series decaying to the single available continuum $2p^6\ ^1S_0$. There are a certain number of peaks common in both spectra of Fig. 4. At nearly 100 eV, the peaks are recognized to be the lowest-energy doublet $1s^2 2p^5 3s^2\ ^2P_J$ decaying to the single available continuum $2p^6\ ^1S_0$. Table V summarizes the identifications for the decay after DC by Ar^{9+} in the energy region below 200 eV where there is nearly overlap of different Auger series. In the energy region between 200 and 252 eV, precise identifications and line attributions are impossible to do: this is understood as due to the overlap of the levels in the series $3p4l,5l$ and $3d4l'$ (Table IV). However, it is clearly seen that the most populated levels belong to the $3pnl$ and $3dn'l'$ series. The highest-intensity peaks point to the center of the DC window, $3p5l$ and $3d4l'$.

V. CONCLUSION

This study has shown that collisions involving open-shell projectiles are particularly difficult to handle: the levels in the exit channels of SC and DC are not well known. This obliges one to perform atomic data determinations. However, the suggested line identifications in the XUV-VUV spectra are consistent with the predictions of the experimental scaling rules. Much is left open for further higher-resolution observations even though important but limited numbers of identifications have been suggested. The important point to be underlined is that, in plasma and beam-foil observations, l statistical population sharing is classically accepted, in the lowest-lying levels; collision-type spectroscopy allows the observation of highly excited levels (Rydberg) where the l sharing is not statistical but, in a given l, the j's are statistically populated. The l sharing changes with the collision velocity. The potentialities of this approach, seen from the point of view of fundamental spectroscopy, seem important for comparing with beam-foil results [38].

calculated transitions should be retained for attribution. These suggested identifications give the complete set of nl populated levels as classically observed in charge-exchange collision spectroscopy. This set is at variance with results of plasma spectroscopy. The $5s\ ^{1,3}P_1^o \rightarrow 2p^6$ transition seen in the x-ray range at 33.56 Å is a branch complemented by the decay in the VUV at 124–125 Å.

One group of large-intensity transitions, at 98.36 and 99.23 Å, are not yet attributed. The nearly equal intensities of the $4d\ ^3F \rightarrow 3p\ ^3D$ and $5s\ ^3P \rightarrow 3p\ ^3D$ are probably related to the direct population mechanism of $n=4$ and 5.

In view of the large number of very low-intensity transitions, some transitions could be present in these different regions due to the decay of some levels populated in DC with large enough fluorescence yields. For example, some decays should feed $2p^5 3s^2\ ^2P_J^o$ since these levels are not directly populated. These observations are, however, difficult to compare to other such observations; we are not aware of other measurements in this XUV-VUV window for neonlike argon in collision processes.

C. Identifications in the Auger spectrum

Comparison of the spectra in Figs. 4(a) and 4(b) clearly shows that the Auger decay following DC by Ar^{9+} is limited to terms energetically below or just on the $3snl$ series limit (at 252 eV, in the emitter frame) (Fig. 7). Higher-lying levels are not expected to decay to $2p^6\ ^1S_0$ but rather to $2p^5 3l$ (this is related to the fact that usually states decay to the closest continuum and the branching ratios for Auger decays are not yet known). They are the closest continua (see Fig.

[1] A. Boileau *et al.*, Plasma Phys. Controlled Fusion **31**, 779 (1989).

[2] (a) G. Bertschinger *et al.*, Phys. Scr. **T83**, 132 (1999); (b) R. Brandenburg, F. Aumayr, G. Petravich, S. Zoletnik, S. Fiedler, K. McCormick, and J. Schweinzer, Fusion Technol. **36**, 289 (1999).

[3] J. B. Greenwood, I. D. Williams, S. J. Smith, and A. Chutjian, Astrophys. J. Lett. **533**, L175 (2000).

[4] V. A. Krasnopolsky and M. J. Mumma, Astrophys. J. **549**, 629 (2001).

[5] C. M. Lisse, D. J. Christian, K. Dennerl, K. J. Meech, R. Petre, H. A. Weaver, and S. J. Wolk, Science **292**, 1343 (2001).

[6] S. Bliman, M. Cornille, B. A. Huber, H. Lebius, A. Langereis, J. Nordgren, and R. Bruch, Phys. Rev. A **60**, 2799 (1999).

[7] S. Bliman, M. Cornille, B. A. Huber, J. Nordgren, and J. E. Rubenson, Phys. Rev. A **63**, 032710 (2001).

[8] C. Harel and H. Jouin, J. Phys. B **25**, 221 (1992).

[9] Z. Chen, C. D. Lin, and N. Toshima, Phys. Rev. A **50**, 511 (1994).

[10] W. Fritsch, J. Phys. B **27**, 3461 (1994).

[11] J. P. Buchet *et al.*, J. Phys. B **20**, 1709 (1987).

[12] C. Jupen, U. Litzen, V. Kaufman, and J. Sugar, Phys. Rev. A **35**, 116 (1987).

[13] (a) P. S. Antsiferov, S. S. Churilov, L. A. Dorokhin, K. N. Koshelev, A. V. Nazarenko, and Yu. V. Sidelnikov, Phys. Scr. **62**, 127 (2000); (b) B. C. Fawcett, A. Ridgeley, and G. E. Bromage, *ibid.* **18**, 315 (1978).

[14] S. Bashkin and J. O. Stoner, *Atomic Levels and Grotrian Diagrams* (North-Holland, New York, 1978), Vol. 2.

[15] R. L. Kelly, J. Phys. Chem. Ref. Data **16**, 403 (1987).

[16] H. L. Zhang, D. H. Sampson, R. E. H. Clark, and J. B. Mann, At. Data Nucl. Data Tables **37**, 17 (1987).

[17] R. Mann, E. Folkmann, and H. F. Beyer, J. Phys. B **14**, 1161 (1981).

[18] R. Hutton, D. Schneider, and M. H. Prior, Phys. Rev. A **44**, 243 (1991).

[19] P. Beiersdorfer, R. E. Olson, G. V. Brown, H. Chen, C. I. Harris, P. A. Neill, L. Schweikhard, S. B. Utter, and K. Widmann, Phys. Rev. Lett. **85**, 5090 (2000).

[20] C. Froese Fisher, Phys. Scr. **T83**, 49 (1999).

[21] S. Bliman, M. Bonnefoy, J. J. Bonnet, S. Dousson, A. Fleury, D. Hitz, and B. Jacquot, Phys. Scr., T **T3**, 63 (1983).

[22] S. Bliman, M. G. Suraud, D. Hitz, B. Huber, H. Lebius, M. Cornille, J. E. Rubensson, J. Nordgren, and E. J. Knystautas, Phys. Rev. A **46**, 1321 (1992).

[23] R. Hutton, M. H. Prior, S. Chanterene, M. H. Chen, and D. Schneider, Phys. Rev. A **39**, 4902 (1989).

[24] S. Bliman, M. Cornille, B. A. Huber, and J. F. Wyart, Phys. Rev. A **56**, 4683 (1997).

[25] W. Eissner, N. Jones, and H. Nussbaumer, Comput. Phys. Commun. **8**, 270 (1974).

[26] R. D. Cowan, *The Theory of Atomic Structure and Spectra* (University of California Press, Berkeley, 1981).

[27] S. Martin, A. Denis, J. Desesquelles, and Y. Ouerdane, Phys. Rev. A **42**, 6564 (1990).

[28] H. Ryufuku, K. Sasaki, and T. Watanabe, Phys. Rev. A **21**, 745 (1980).

[29] A. Barany *et al.*, Nucl. Instrum. Methods Phys. Res. B **9**, 397 (1985).

[30] A. Niehaus, J. Phys. B **19**, 2925 (1986).

[31] K. Okuno, in *The Physics of Electronic and Atomic Collisions*, edited by L. J. Dubé, J. B. A. Mitchell, J. W. McConkey, and C. E. Brion, AIP Conf. Proc. No. 360 (AIP, Woodbury, NY, 1995), pp. 870–876.

[32] R. E. Olson and A. Salop, Phys. Rev. A **16**, 531 (1977).

[33] R. K. Janev, Phys. Lett. A **160**, 67 (1991).

[34] K. Dimitriou, Ph.D. thesis, Orsay, France, 2001.

[35] J. Vancura, V. J. Marchetti, J. J. Perotti, and V. O. Kostroun, Phys. Rev. A **47**, 3758 (1993).

[36] S. Bliman, M. G. Suraud, D. Hitz, J. E. Rubensson, J. Nordgren, M. Cornille, P. Indelicato, and E. J. Knystautas, J. Phys. B **22**, 3647 (1989).

[37] W. L. Wiese and G. A. Martin, in *A Physicist's Desk Reference*, edited by H. L. Anderson (AIP, New York, 1989), p. 92.

[38] E. J. Knystautas and S. Bliman, Phys. Scr. **T40**, 65 (1992).